![Northwell Health logo]

2015

Inner Segment Remodeling and Mitochondrial Translocation in Cone Photoreceptors in Age-Related Macular Degeneration With Outer Retinal Tubulation

K. M. Litts

J. D. Messinger

K. B. Freund
Northwell Health

Y. Zhang

C. A. Curcio

Recommended Citation

Inner Segment Remodeling and Mitochondrial Translocation in Cone Photoreceptors in Age-Related Macular Degeneration With Outer Retinal Tubulation

Katie M. Litts,[1,2] Jeffrey D. Messinger,[1] K. Bailey Freund,[3] Yuhua Zhang,[1] and Christine A. Curcio[1]

[1]Department of Ophthalmology, University of Alabama School of Medicine, Birmingham, Alabama, United States
[2]Vision Science Graduate Program, University of Alabama at Birmingham, Birmingham, Alabama, United States
[3]Vitreous Retina Macula Consultants of New York, New York City, New York, United States

Correspondence: Christine A. Curcio, Department of Ophthalmology, EyeSight Foundation of Alabama Vision Research Laboratories, University of Alabama School of Medicine, 1670 University Boulevard Room 360, Birmingham, AL 35294-0099, USA;
curcio@uab.edu.

PURPOSE. To quantify impressions of mitochondrial translocation in degenerating cones and to determine the nature of accumulated material in the subretinal space with apparent inner segment (IS)-like features by examining cone IS ultrastructure.

METHODS. Human donor eyes with advanced age-related macular degeneration (AMD) were screened for outer retinal tubulation (ORT) in macula-wide, high-resolution digital sections. Degenerating cones inside ORT (ORT cones) and outside ORT (non-ORT cones) from AMD eyes and unaffected cones in age-matched control eyes were imaged using transmission electron microscopy. The distances of mitochondria to the external limiting membrane (ELM), cone IS length, and cone IS width at the ELM were measured.

RESULTS. Outer retinal tubulation and non-ORT cones lose outer segments (OS), followed by shortening of IS and mitochondria. In non-ORT cones, IS broaden. Outer retinal tubulation and non-ORT cone IS myoids become undetectable due to mitochondria redistribution toward the nucleus. Some ORT cones were found lacking IS and containing mitochondria in the outer fiber (between soma and ELM). Unlike long, thin IS mitochondria in control cones, ORT and non-ORT IS mitochondria are ovoid or reniform. Shed IS, some containing mitochondria, were found in the subretinal space.

CONCLUSIONS. In AMD, macula cones exhibit loss of detectable myoid due to IS shortening in addition to OS loss, as described. Mitochondria shrink and translocate toward the nucleus. As reflectivity sources, translocating mitochondria may be detectable using in vivo imaging to monitor photoreceptor degeneration in retinal disorders. These results improve the knowledge basis for interpreting high-resolution clinical retinal imaging.

Keywords: age-related macular degeneration, cones, ellipsoid, histology, Müller cells, myoid, outer retinal tubulation, photoreceptors, transmission electron microscopy

The most apparent clinical and histological pathology of age-related macular degeneration (AMD) occurs in the retinal pigment epithelium (RPE) and Bruch's membrane and in the adjacent subretinal space and choroid, yet ultimately, vision is lost due to degeneration and death of photoreceptors. To date, histological studies of AMD eyes have demonstrated that photoreceptors have shortened outer segments (OS) and inner segments (IS),[1] redistributed cone opsin,[2] and stress protein expression; cells dwindle in number over drusen[3] and undergo apoptosis.[4] A gliotic formation of cone photoreceptors and Müller cells in interconnecting tubes, known as outer retinal tubulation (ORT), was originally seen over disciform scars.[5] With advances in high-resolution imaging such as spectral-domain optical coherence tomography (SD-OCT), in vivo retinal imaging is revealing new insights into photoreceptor degeneration in AMD and other retinal disorders. As visualized by SD-OCT, ORT are branching tubular structures in the outer nuclear layer that appear as hyporeflective areas surrounded by a hyperreflective border that corresponds to the IS and external limiting membrane (ELM).[6,7] Adaptive optics-assisted retinal imaging, such as adaptive optics scanning laser ophthalmoscopy (AOSLO),[8] has been used to demonstrate changes in cone spacing and cone reflectivity in inherited retinal diseases,[9] geographic atrophy of AMD,[10] and association with subretinal drusenoid deposits (SDD).[11]

Photoreceptor reflectivity captured by high-resolution imaging devices can originate from scattering at refractive index boundaries and from waveguiding.[12,13] Photoreceptors have unique tightly bundled IS mitochondria comprising 75% of normal IS ellipsoid (ISel) volume.[14] In addition to efficiently using high oxygen levels of choroidal origin for phototransduction, mitochondria possibly contribute to IS optical properties, because they are light scatterers.[13,14] In SD-OCT, the second of four outer retinal hyperreflective bands, called the ellipsoid zone, has been attributed in part to mitochondria of the photoreceptor ISel,[15] yet this attribution is debated.[16] Mitochondrial morphology is dynamically controlled to respond to energy needs and environmental stimuli. Refractivity of isolated mitochondria is affected by their metabolic state, at least in vitro.[17]

The significance of reflectivity changes in high-resolution imaging may be elucidated with new information afforded by the higher magnification and resolution provided by histological and ultrastructural investigation. For high-resolution imaging such as AOSLO to achieve maximal utility for photoreceptor structure in AMD progression, it is important to understand the photoreceptor ultrastructure, including mitochondria, which may contribute to hyperreflectivity in various retinal imaging modalities. Histology of AMD is particularly possible, because this disease is widely prevalent among the elderly.[18] Many short postmortem eyes were screened for advanced AMD and processed for histology in creating Project MACULA, an online digital microscope (http://projectmacula.cis.uab.edu/). Although many studies describe photoreceptor degeneration in AMD (see Supplementary Table S1),[1-5,19-22] none extensively describe cone degeneration with a focus either on the IS or advanced AMD. The purposes of this study were to survey cone degeneration in late AMD, to examine cone IS ultrastructure with transmission electron microscopy (TEM) in order to quantify impressions of mitochondrial translocation in degenerating cones, and to assess the identity of accumulated material with apparent IS-like features in the subretinal space. These observations will contribute to knowledge of the ultrastructural and molecular basis of clinical imaging.

METHODS

Eyes

This research adhered to the tenets of the Declaration of Helsinki and was approved by the Institutional Review Board at the University of Alabama at Birmingham. Human donor eyes with gross macular appearance consistent with AMD were obtained from the Alabama Eye Bank for research purposes, with a median death-to-preservation time of 2 hours 40 minutes. Eyes were preserved in 1% paraformaldehyde and 2.5% glutaraldehyde in 0.1 M phosphate buffer after anterior segment removal and were stored in this fixative until used. Tissue was postfixed by osmium tannic acid paraphenylenediamine to accentuate extracellular neutral lipids[23,24] and embedded in epoxy resin (Polybed 812; Polysciences, Warrington, PA, USA). Macula-wide, 0.8 μm-thick horizontally oriented sections[25,26] through the foveola and at 2 mm superior to the foveal center (near the rod peak[27]) were stained with toluidine blue.

Age-related macular degeneration case ascertainment was made using published histological criteria.[26,28,29] Macula-wide sections were imaged with a 60× oil-immersion objective (numerical aperture = 1.4) and a digital camera (model XC10; Olympus, Tokyo, Japan). Sections were reviewed in a systematic and unbiased manner.[26] Scanned histological sections are available online at http://projectmacula.cis.uab.edu/. In late AMD eyes (40 exudative AMD, 13 geographic atrophy [GA]) from nondiabetic Caucasian donors, 77 ORT were identified in macula-wide high-resolution sections as described below. Eyes containing apparent, well-preserved mitochondria were selected for further investigation. Cones in 25 eyes (18 exudative AMD, 1 GA, 1 RPE hyperplasia of uncertain origin; 84.4 ± 5.2 years of age; 12 females, 8 males) and 5 eyes with unremarkable pathology serving as controls (86.0 ± 3.7 years of age; 4 females, 1 male) were imaged by TEM.

Imaging by Transmission Electron Microscopy

Eyes were sectioned at silver-gold thickness and viewed with a model 1200 EXII electron microscope (JEOL, Peabody, MA, USA) and imaged with an AMTXR-40 camera (Advanced Microscopy Techniques, Danvers, MA, USA). Here, we report single-section TEM and deduced the three-dimensional organelle shape of mitochondria (i.e., circular cross-sections were deduced as having derived from spherical mitochondria). Not all ORT selected by light microscopy were imaged, because only one 2-mm region of interest in each 8-mm section fit on a TEM grid. Any ORT in that region of interest was imaged even if not the original identified ORT of interest. By en face OCT, ORT are interconnected, suggesting that they will have a unified and smoothly transitioning microscopic luminal structure.[6,30]

Cones selected for TEM imaging contained nucleated cell bodies continuous with the IS through the ELM. Cones located in ORT were considered ORT cones (45 ORT in 12 eyes) for the purposes of analysis. Degenerating cones located outside an ORT and within the remaining mosaic where the ELM was continuous and flat were considered non-ORT cones. Material with IS-like properties located in the subretinal space was designated as Shed IS for reasons provided in the Results. All images were composited with adjustments for exposure, contrast, and background correction only (Photoshop versions CS5 Extended and CS6; Adobe Systems, San Francisco, CA, USA).

Measurements

Measurements from ImageJ software (http://imagej.nih.gov/ij/; provided by the National Institutes of Health, Bethesda, MD, USA) are illustrated in Figure 1. Mitochondria distance (Mito distance) was defined as the average distance from the centroid of each mitochondrial cross-section to the ELM for each cone. Mitochondria in the IS were assigned positive distances, and mitochondria internal to the ELM in the outer fiber[31] and near the nucleus were assigned negative distances, relative to the ELM. Cone IS length was measured from the ELM to the apex of the IS near the OS. Cone width was measured at the ELM. Cone IS myoid (ISmy) length was measured from the ELM to the top of the mitochondria. Cone ISmy was measured in Control cones from unremarkable eyes only, because it was not detectable in every degenerating cone, due to mitochondrial redistribution, as shown in the Results.

Statistical Analysis

One-way analysis of variance (ANOVA) was performed between groups of cones (ORT, non-ORT, Controls) for each of the measurements to test whether at least one mean was different at the α significance of <0.05, under the null hypothesis that all cones had the same dimensions. Post hoc Tukey's Honestly Significant Difference test was performed to determine which group means were statistically significant. Statistical analysis was performed using Matlab software (MathWorks, Natick, MA, USA).

RESULTS

Comparison of Unaffected Cones and Degenerating Cones

For reference, a normal cone from a healthy macula is shown with a long IS containing mitochondria in the ISel that are thin and tightly packed (Fig. 2A). The ISmy is located internal to the ISel. Degenerating non-ORT cones have an IS that is shortened and broadened, with ovoid mitochondria (Fig. 2B). Degenerating cones in mature phase[7] of a closed ORT likewise have shrinking IS (Fig. 2C). Degenerating ORT and non-ORT cones with varying IS lengths were imaged at different stages of
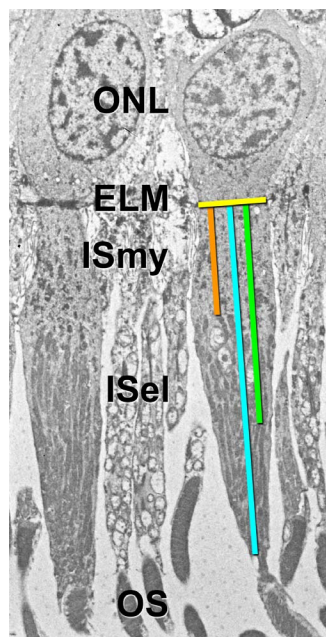
FIGURE 1. Cone with ultrastructure measurements illustrated. Cone width was measured at the ELM (*yellow line*). Mito distance is the average distance from the centroid of each mitochondrion in the IS to the ELM in each cone (*green line*). Cone IS length was measured from the ELM to the apex of the IS (*blue line*). Cone ISmy was measured from the ELM to the top of the ISel and was measured only in Control cones as shown here (*orange line*). Photoreceptor inner segment myoid was not measurable in degenerating cones. Image shows the same cone as Figure 2A. ONL, outer nuclear layer; ELM, external limiting membrane; ISmy, photoreceptor inner segment myoid; ISel, photoreceptor inner segment ellipsoid; OS, photoreceptor outer segment.

degeneration but contained mitochondria with similar morphology.

Degenerating ORT Cones

Degenerating cones with long IS (Fig. 3A) contained spherical mitochondria (Fig. 3A, inset) that had not moved internal to the ELM toward the nucleus. During the degeneration process, ORT cone nuclei retract from the ELM, resulting in an elongated outer fiber (Fig. 3B). In these cones, mitochondria are small, with some internal to the ELM, resulting in a lack of visible myoid (Fig. 3B, inset). In addition, in a mature phase[7] ORT, cones with different IS lengths can be found next to each other (Fig. 3C). Again, these degenerating ORT cones contain small and spherical mitochondria (Fig. 3C, inset). In another ORT, cones were found on the scleral side with stubby IS pointed into the lumen, which contains Shed IS (described below) (Fig. 3D). In addition to spherical mitochondria, some cones also contain heterogeneous electron-dense inclusions considered to be lipofuscin, previously described in normal cone photoreceptors.[32–35] An example of ORT at a mature phase[7] is shown in Figure 3E for reference.

Degenerating Non-ORT Cones

Non-ORT cones as defined in the Methods were imaged at various stages of degeneration. Degenerating non-ORT cones with long IS have small, ovoid mitochondria that have moved in the direction of the ELM, leaving the IS apex devoid of any visible organelles (Fig. 4A). In contrast, despite having a shortened IS, the cone in Figure 4B still has a remnant OS
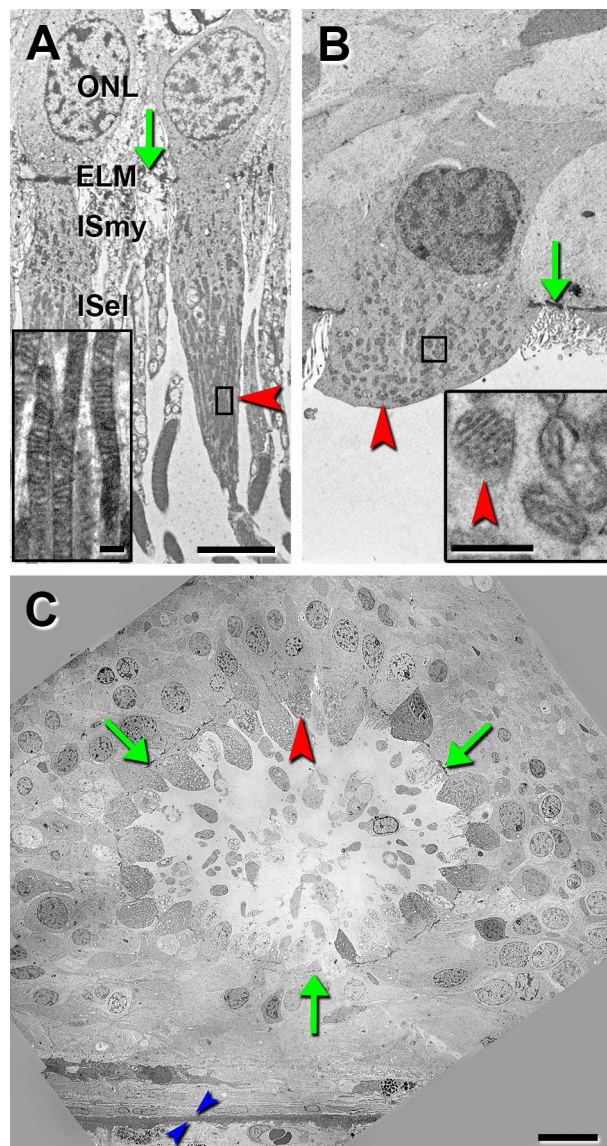

FIGURE 2. Comparison of unaffected cones, degenerating non-ORT cones, and degenerating ORT cones. Neovascular AMD, except where noted. *Green arrows* indicate ELM, and *red arrowheads* indicate mitochondria in all panels. (**A**) Photoreceptors at 2.5 mm temporal to the foveal center in a healthy macula. Mitochondria are thin and tightly packed in the ISel (*inset*, magnified box). Eighty-five-year-old female donor. (**B**) Degenerating non-ORT cone at 3 mm from the foveal center. Mitochondria are spherical, ovoid, or reniform (*inset*, magnified box). Eighty-seven-year-old female donor. (**C**) Mature closed ORT containing cones with shrinking inner segments at 1.2 mm temporal from the foveal center. The ELM delimits the ORT lumen. Bruch's membrane (*blue arrowheads*). Seventy-nine-year-old male donor. ELM, external limiting membrane; ISel, photoreceptor inner segment ellipsoid; ISmy, photoreceptor inner segment myoid; ONL, outer nuclear layer. *Scale bars*: 5 μm (**A**, **B**); 20 μm (**C**); 250 nm (*insets*).

attached, and the cone is wider than the cones in Figure 4A. The cone contains reniform mitochondria that are sparse, and a cluster of mitochondria has translocated near the nucleus (Fig. 4B, inset). In addition, cones lacking OS can have a layer of mitochondria above a devoid IS apex (Fig. 4D). This may contribute to Shed IS (discussed below). Cones with shortened IS and lacking OS contain both spheroid and reniform mitochondria (Fig. 4E). Degenerating cones found over a
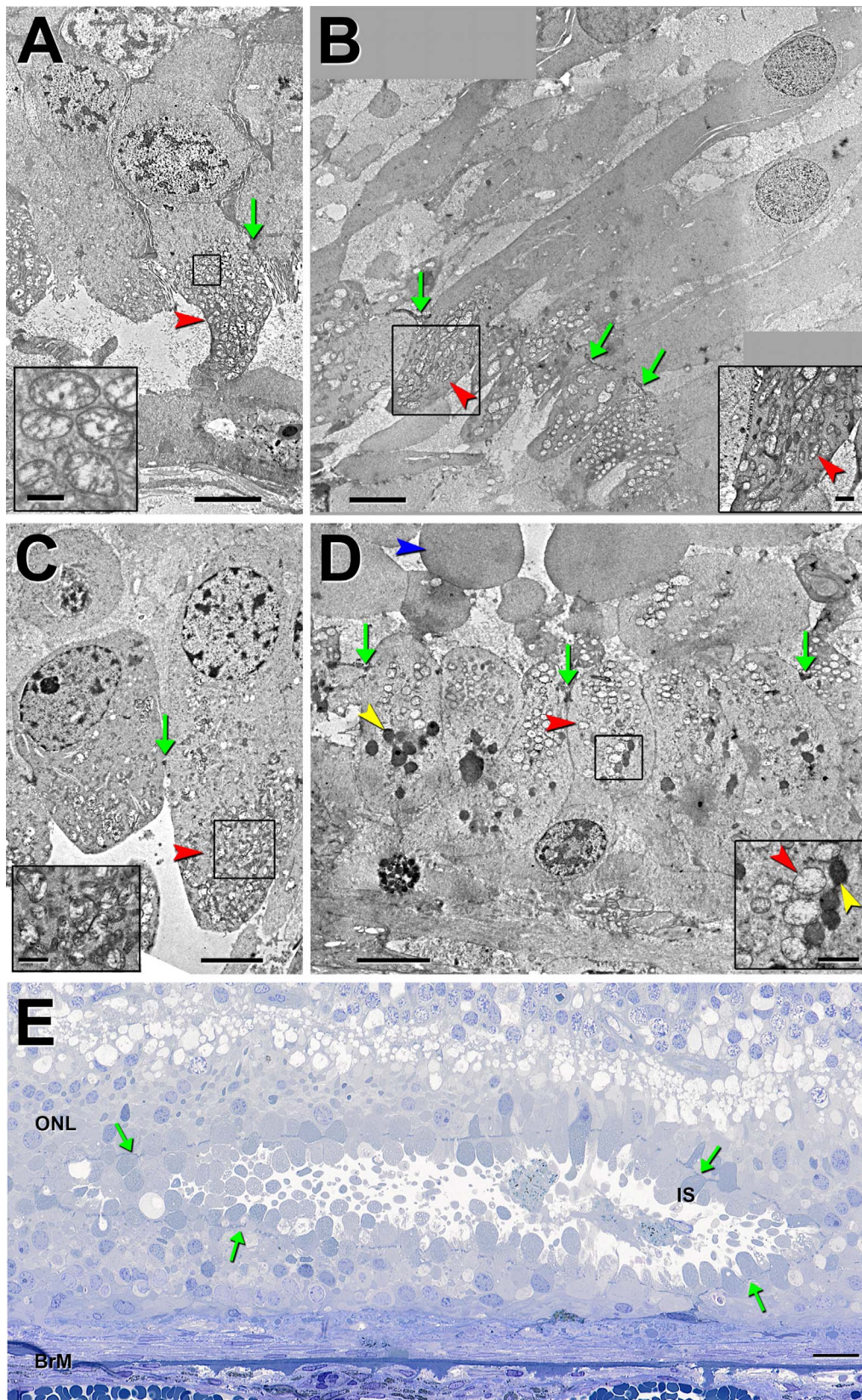
FIGURE 3. Cone degeneration and mitochondria in ORT of neovascular AMD eyes. *Green arrows* indicate ELM, and *red arrowheads* indicate mitochondria in all panels. (**A**) Outer retinal tubulation cone with long IS containing spherical mitochondria that have not translocated internally to the ELM (*inset*, magnified box). At 2.1 mm temporal from the foveal center. Seventy-seven-year-old male donor. (**B**) Cone from mature[7] ORT with nucleus retracted from ELM. Mitochondria in IS are ovoid (*inset*, magnified box). At 2 mm nasal from the foveal center. Eighty-seven-year-old female donor. (**C**) Cones at the mature stage of degeneration in a closed ORT.[7] Mitochondria are small and spherical (*inset*, magnified box). At 2.3 mm nasal from the foveal center. Seventy-nine-year-old male donor. (**D**) Cones on the scleral side of the degenerate phase, closed ORT containing translocated

mitochondria (*inset*, magnified box), and cone lipofuscin (*yellow arrowhead*). Shed IS in the lumen above the cones (*blue arrowhead*). At 2 mm nasal from the foveal center. Eighty-seven-year-old female donor. (E) High-resolution histology section from a mature[7] ORT. External limiting membrane encircles the closed ORT. Cones have IS. Retinal pigment epithelium and other contents are seen in lumen. Cones in (C) are from this ORT. BrM, Bruch's membrane. IS, photoreceptor inner segment; ONL, outer nuclear layer. *Scale bars*: 5 μm (A–D); 20 μm (E); 1 μm (*inset*).

hemorrhage in the subretinal space also contain translocated mitochondria, although sparse (Fig. 4C).

Measurements

Cone ultrastructure measurements include Mito distance, cone IS length and width in degenerating non-ORT and ORT cones, and cone ISmy in Control cones (Fig. 5). Compared to ORT cone IS length (7.1 ± 5.4 μm), non-ORT cone IS length (13.3 ± 8.3 μm), and Control cone IS length (24.8 ± 4.1 μm) are both longer. In ORT cones, mitochondria are closer to the ELM (1.7 ± 3.0 μm) than in Control cones (12.9 ± 4.9 μm) or non-ORT cones (7.1 ± 3.1 μm). Degenerating non-ORT cones were wider at the ELM (6.3 ± 3.2 μm) than Control cones (4.9 ± 1.1 μm). All three cone types differed significantly for Mito distance and cone IS length. However, the ORT cone width (5.7 ± 2.1 μm) was not significantly different from Control or non-ORT cone width. Cone ISmy length in Control cones was 5.2 ± 1.7 μm. Cone ISmy was measured in unaffected cones from unremarkable eyes only, because the redistribution of mitochondria within degenerating cones rendered the ISmy undetectable.

Shed IS

In the course of this systematic review of well-preserved late AMD eyes, many with attached retinas, material with IS-like properties was found within the subretinal space and interspersed with sloughed, rounded RPE (Fig. 6A). Shed IS were found in 8 (44.4%) of the 18 neovascular AMD eyes imaged by TEM. Shed IS may be a process in cone degeneration. By viewing serial cross-section images in Figure 7, a cone can be seen shedding part of its IS into the subretinal space. Shed IS can contain small and spheroid mitochondria (Figs. 6B–D, insets). The mitochondria in Shed IS can form a cluster (Figs. 6B, 6C) or completely fill the IS material (Fig. 6D). Other Shed IS have a finely textured cytosol lacking visible organelles (Fig. 3D, blue arrowhead). We also found a cone IS apex devoid of mitochondria, with a cushion of mitochondria closer to the ELM (Fig. 4D) in an eye that also had Shed IS. This configuration may be a precursor to Shed IS.

Shed IS are distinguishable from SDD, also in the subretinal space, by its ultrastructure (Fig. 8). SDD have been described as drusenoid dollops with a granular internal structure containing unesterified cholesterol.[36,37] Photoreceptors over Shed IS are lacking OS, whereas photoreceptors overlying SDD are more likely to have OS, although shortened.

DISCUSSION

Reflectivity of Degenerating Cone Photoreceptors

Our results provide a basis for improved interpretation of high-resolution retinal imaging including SD-OCT and AO-assisted imaging modalities such as AO-OCT[38–43] and AOSLO.[44–47] As seen by SD-OCT, a timeline of photoreceptor degeneration based on the disappearance of hyperreflective outer retinal bands[48] is consistent with our ultrastructural observations of cone degeneration, where cones lose OS, followed by IS shortening and mitochondrial translocation. The proposed order of photoreceptor degeneration starts with OS shortening as seen by absent band 3 (interdigitation zone), followed by band 2 (ellipsoid zone) disruption, and finally loss of band 1

(ELM).[15,48] Although degenerating cones lose OS early like degenerating rods, ORT cones, which can survive for extended periods,[49] do so largely without OS.[7] As seen in end-stage phase ORT, the ELM is still present when recognizable photoreceptors are absent, suggesting remarkable persistence of Müller cells and a final source of reflectivity associated with cone degeneration.[7]

A previous SD-OCT study showing decreased thickness from the outer plexiform layer to band 3 over drusen suggests a degenerative process in AMD.[50] In addition, as seen by SD-OCT, photoreceptors degenerating over small choroidal melanoma have been described as shaggy[51] (i.e., irregular, swollen, and elongated). By AOSLO, reduction in cone reflectivity over drusen and at the edge of GA even when band 2 was visible on SD-OCT[10] may provide insight into cone degeneration. Hyporeflective cones at the edge of GA seen by AOSLO may show evidence of reduced waveguiding but still contain sources of IS reflectivity.[10] Recently, a model developed by Zayit-Soudry et al.[10] to explain observations made with AOSLO and SD-OCT in AMD showed cones thinning and retaining OS as they degenerated. Our current and published observations of short, broadened cone IS[5] and animal models of photoreceptor degeneration do not support that interpretation.

In our separate publications, we proposed, on the basis of histology and TEM, that the reflective ORT border can be accounted for by a combination of ELM and IS mitochondria translocated to the same level as the ELM by atrophy of IS.[7,52] In addition, we showed a direct clinicopathologic correlation between clinical SD-OCT and histology of ORT in one AMD case, establishing mitochondria as the organelle present in shrinking cone IS.[52] These data suggest that mitochondria are independent reflectivity sources even when cones are severely misaligned, as waveguiding seems unlikely where cones are radially aligned around ORT lumens. Scattering of light by persisting mitochondria could help explain the hyperreflective ORT border seen in SD-OCT, lacking OS.[7] Previous studies using cell culture and isolated mitochondria models suggest that mitochondria are strong light scatterers. Furthermore, light scattering by mitochondria changes when undergoing oxidative stress due to morphology and refractivity changes.[53,54] Together with IS mitochondria, the ELM may contribute to reflectivity of degenerating non-ORT cones. The ELM of apparent ORT exhibits immunoreactivity for ICAM-1, indicating tissue injury and inflammation at this site.[55] Thickening of the ELM band is seen on SD-OCT of patients with achromatopsia, a progressive cone degeneration,[56] and Stargardt disease, caused by a dysfunctional ABCA4 protein.[57,58] These reflectivity changes may signify mitochondria that are translocating, gliosis of Müller cells,[58] as-yet-unidentified ultrastructural alterations to junctional complexes, or a combination. Altered hyperreflectivity in SD-OCT related to mitochondria location may be good indicators of photoreceptor health. Thus, the distance between the ellipsoid zone and ELM may be an additional SD-OCT marker, which may be imaged with improved spatial resolution for cone degeneration.

Cone Degeneration

The ability to target specific cell types and organelles like we can in histology and TEM is currently not yet possible by
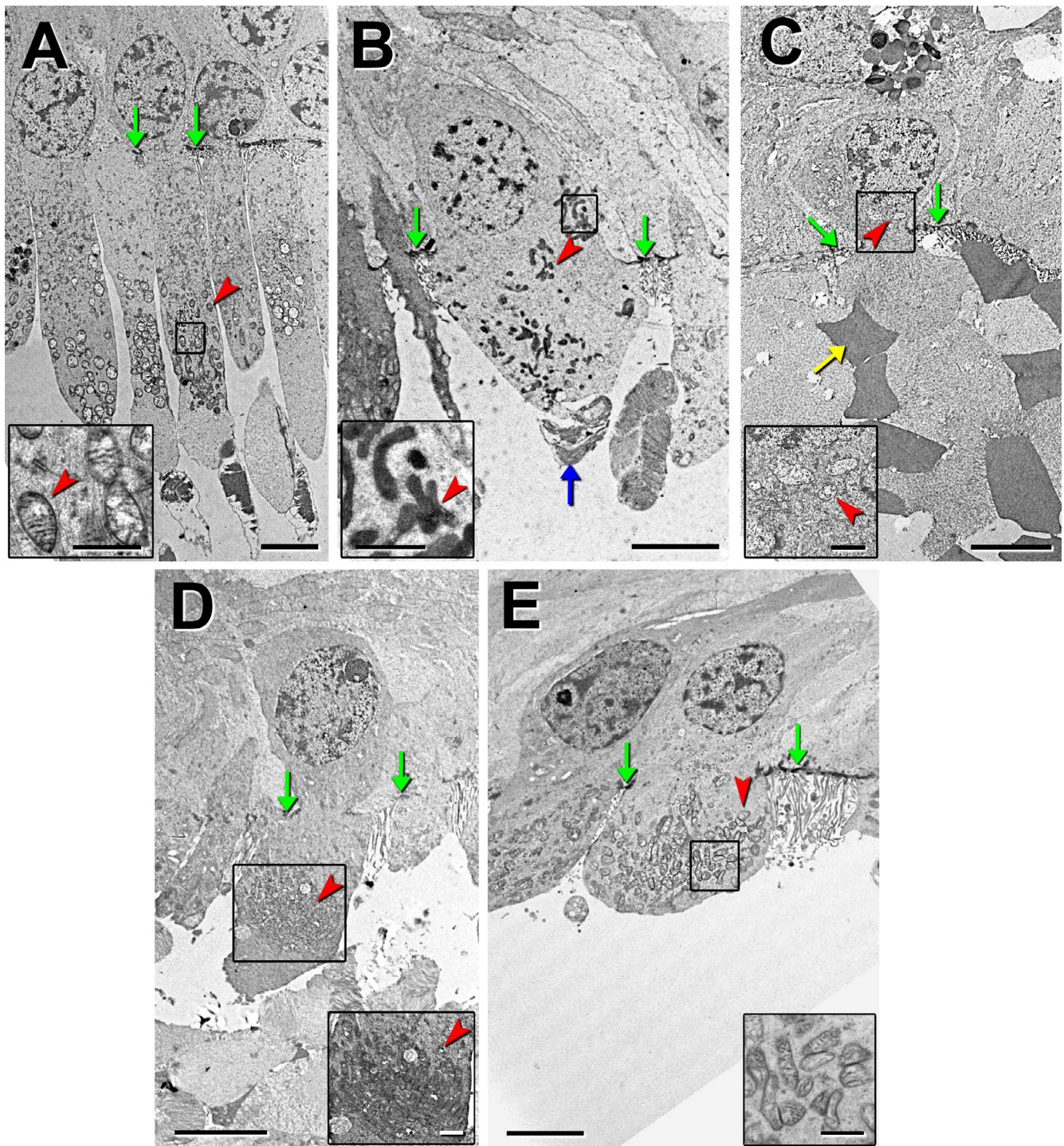
FIGURE 4. Mitochondria in degenerating non-ORT cones. Neovascular AMD, except where noted. *Green arrows* indicate ELM, and *red arrowheads* indicate mitochondria in all panels. (**A**) Non-ORT cones with long IS and OS. Mitochondria (*inset*, magnified box) are small, ovoid, and translocated in direction of the ELM leaving the IS apex devoid of any visible organelles. 0.7 mm nasal from the foveal center. Eighty-eight-year-old male donor. RPE hyperplasia of uncertain etiology. (**B**) Non-ORT cone with shortened IS and remnant OS (*blue arrow*). Mitochondria are sparse, and a cluster has translocated near the nucleus (*inset,* magnified box). At 3 mm from the foveal center. Seventy-seven-year-old female donor. (**C**) Non-ORT cone containing sparse mitochondria (*inset*, magnified box), found over a hemorrhage in subretinal space (erythrocyte, *yellow arrow*). At 1.8 mm temporal from the foveal center. Eighty-three-year-old female donor. (**D**) Non-ORT cone with cushion of mitochondria in IS (*inset*, magnified box). At 3 mm nasal from the foveal center. Eighty-three-year-old female donor. (**E**) Non-ORT cones with shortened IS containing spherical and kidney shaped mitochondria (*inset*, magnified box). At 3 mm from foveal center. Eighty-seven-year-old female donor. *Scale bars*: 5 μm; 1 μm (*inset*).
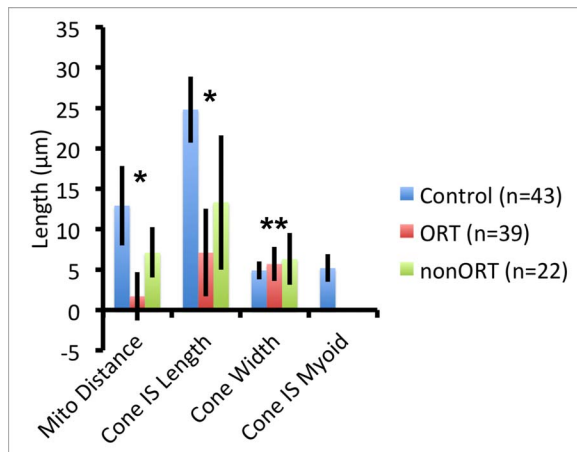
FIGURE 5. Cone ultrastructure measurements. Mitochondria distance (Mito distance), cone IS length, cone width, and cone IS myoid are means ± standard deviations (*error bars*). Cone IS myoid was measured in Control cones only because the dispersion of mitochondria within degenerating cones made myoids indistinguishable. *n*, number of cones. ANOVA. *$P < 0.001$; **$P = 0.24$.

clinical imaging. We observed that during cone degeneration, cones lose their OS, followed by IS shortening, which have also been observed in other histological studies (summarized in Supplementary Table S1). What our study newly reveals is that

mitochondria migrate in the IS and outer fiber toward the nucleus, whereas some mitochondria are sequestered in Shed IS, sloughed off into the subretinal space. ORT and non-ORT cones degenerate in a similar but not identical fashion. Degenerating non-ORT cones are wider at the ELM than the degenerating ORT cones. Outer retinal tubulation cones may be restricted by the ELM from broadening due to space or curvature constraints related to the ELM. Degenerating non-ORT cones are located where the ELM is flat and can expand in width with fewer restrictions. Cone IS shortening and loss of detectable myoid is part of cone degeneration. Stunted, wide cones, not part of an ORT, have previously been described in AMD.[5,59]

The material with IS properties in the subretinal space that we designated Shed IS may be a process in cone degeneration. As cones degenerate, IS shorten, perhaps by sloughing parts of the IS into the subretinal space. Depending on how the mitochondria migrate in the IS, Shed IS may or may not contain mitochondria. Shed IS were not found in all neovascular AMD eyes examined here. Why some cones Shed IS and others do not remains to be elucidated. Because we used single-section histology and TEM of advanced AMD, we may have missed Shed IS in sections not examined, or macrophages or microglia may have already cleared them. Fragmented mitochondria in cytoplasmic vacuoles have been observed undergoing extrusion from apoptotic cells, or a process called mitoptosis, in cell culture models inducing perinuclear mitochondria producing increased reactive oxygen species (ROS).[60,61] A similar process may be occurring in photoreceptors, resulting in Shed IS.
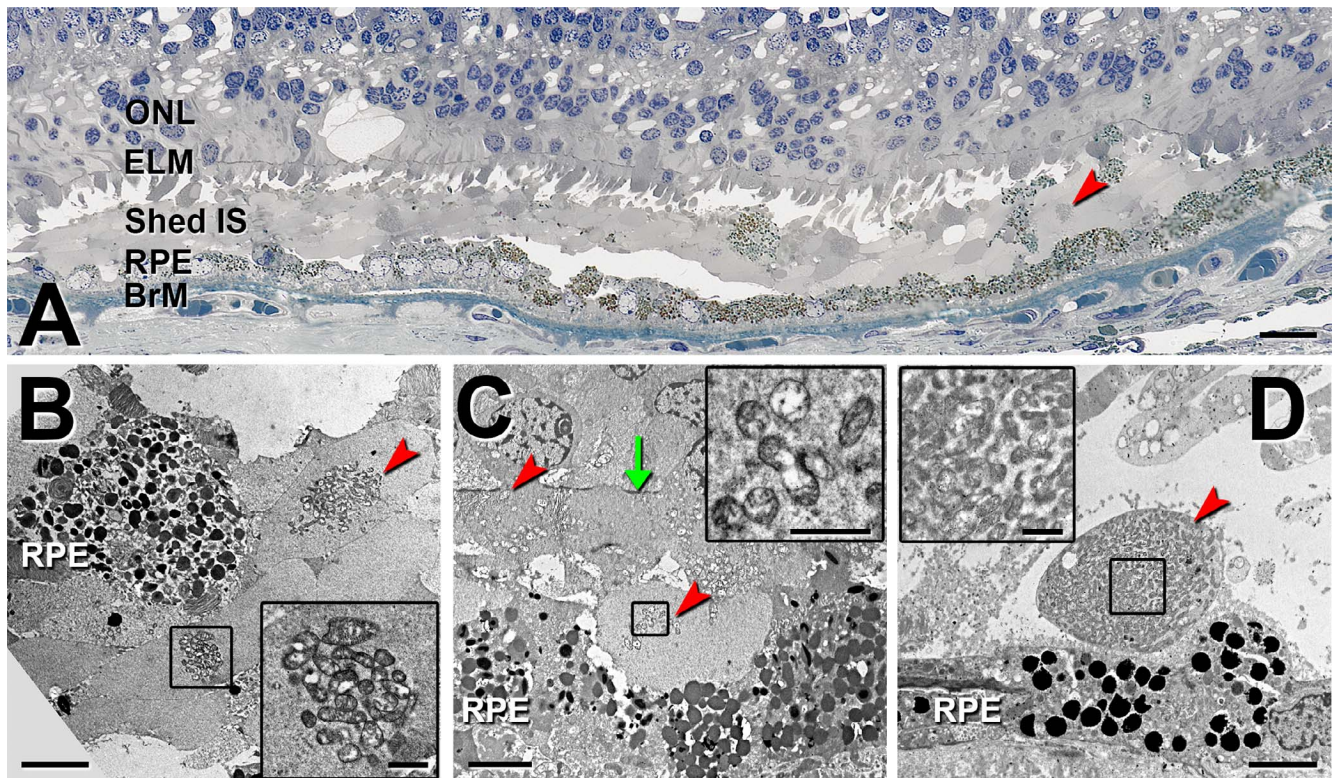

FIGURE 6. Mitochondria in Shed IS in neovascular AMD. (**A**) Shed IS in subretinal space interspersed with RPE sloughed from subjacent monolayer. At 3 mm nasal from the foveal center; 0.8-µm section with toluidine blue stain. Seventy-nine-year-old male donor. (**B**) Shed IS between RPE cells. Some Shed IS contain mitochondria (*red arrowhead, inset*, magnified box). Other Shed IS have finely textured cytosol-lacking visible organelles. At 3 mm nasal from the foveal center. Eighty-three-year-old female donor. (**C**) Shed IS containing a cluster of mitochondria (*inset*, magnified box) below non-ORT cones. ELM (*green arrow*). At 2.5 mm temporal from the foveal center. Seventy-six-year-old male donor. (**D**) Shed IS filled with mitochondria (*inset*, magnified box) found on top of the RPE in subretinal space. At 2.1 mm temporal from the foveal center. Seventy-nine-year-old male donor. BrM, Bruch's membrane; ELM, external limiting membrane; IS, photoreceptor inner segment; ONL, outer nuclear layer; RPE, retinal pigment epithelium. *Scale bars*: 20 µm (**A**); 5 µm (**B–D**); 1 µm (*inset*).
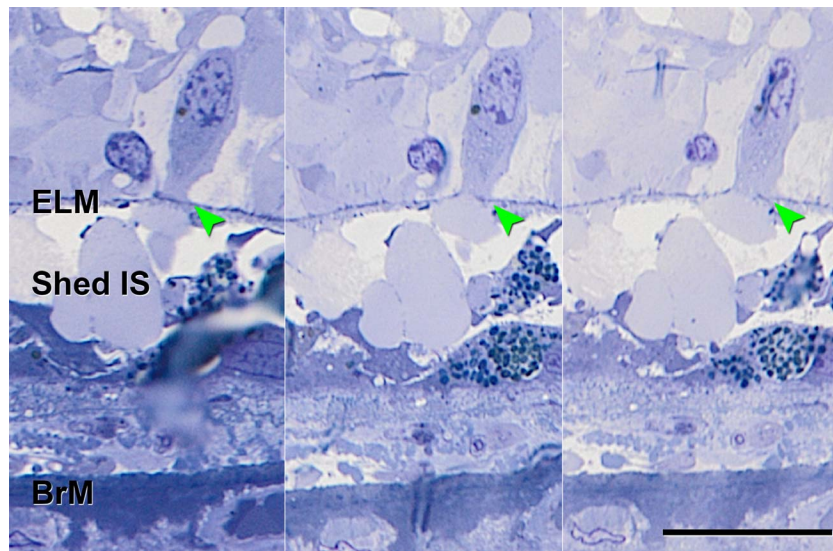
FIGURE 7. Cone IS shedding series. Three panels showing serial high-resolution histology sections of a cone shedding part of its IS. Changes in ELM and cone size are indicated by a *green arrowhead*. BM, Bruch's membrane; ELM, external limiting membrane; IS, photoreceptor inner segment. At 3.5 mm nasal from foveal center. Ninety-year-old female donor. Neovascular AMD. *Scale bar*: 20 μm.

Additionally, Shed IS may be one of several reflectivity sources in the subretinal space, along with RPE, SDD, and intact photoreceptors.

Mitochondria in Degenerating Neurons

Although our data are morphological, they are relevant to understanding subcellular mechanisms of cone degeneration potentially accessible in vivo via high-resolution imaging. The change in IS mitochondrial morphology from long and thin in Control cones to small, ovoid, and reniform in degenerating cones was striking and suggests major functional change in these cells. Mitochondria are essential to oxidative phosphorylation, intermediary metabolism, calcium buffering, redox signaling, and apoptosis regulation, and are increasingly seen as central to neurodegeneration.[62–70] Changes in all of these processes including bioenergetic failure may contribute to cell death in age-related neurodegenerations.[69,71] Reactive oxygen species are constantly generated by oxidative phosphorylation. When levels exceed the limits of what is useful for intracellular
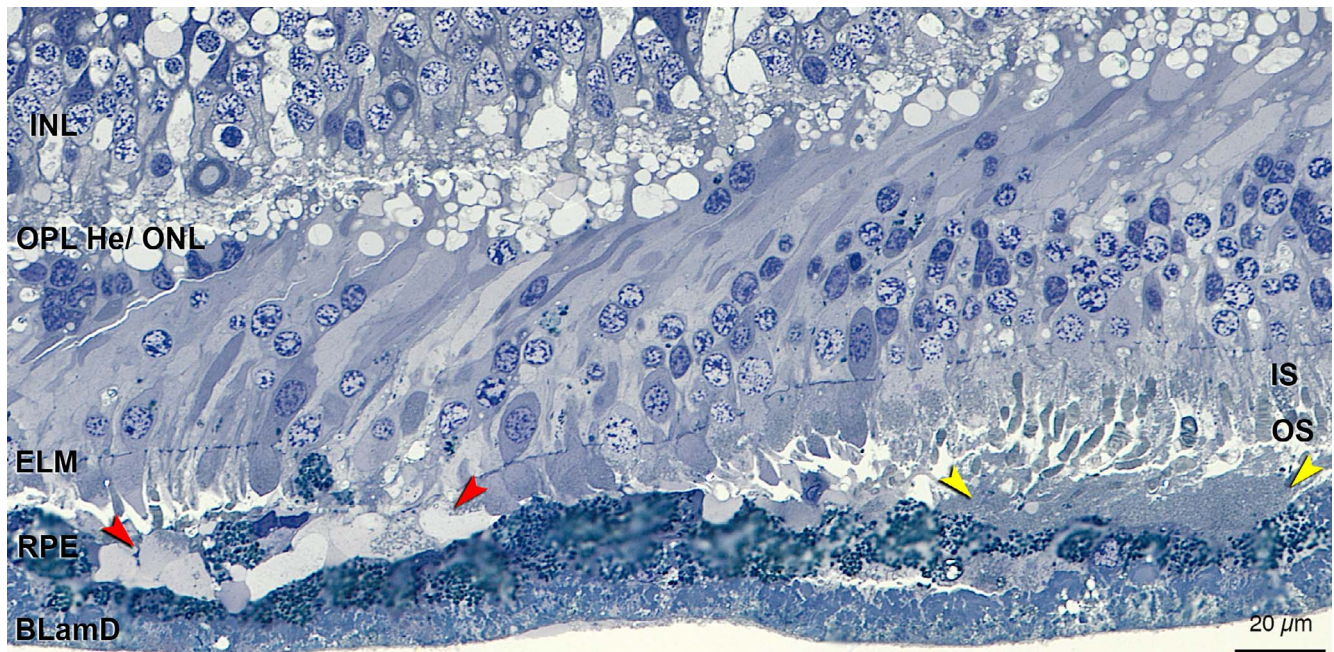

FIGURE 8. Shed IS in subretinal space can be distinguished from subretinal drusenoid deposit (SDD). Shed IS on left (between *red arrowheads*) with overlying degenerating non-ORT cones. Subretinal drusenoid deposit on right (between *yellow arrowheads*) with overlying photoreceptors containing OS. OPL He/ONL, ectopic photoreceptor nuclei are found translocated along the Henle fibers, blurring the division between the outer plexiform layer and outer nuclear layer at the nasal end of the section. At 3.3 mm temporal from foveal center. Ninety-four-year-old female donor. Neovascular AMD. OPL He/ONL, outer plexiform layer, Henle fibers/outer nuclear layer; ELM, external limiting membrane; INL, inner nuclear layer; RPE, retinal pigment epithelium; BLamD, basal lamanar deposit.

signaling, ROS can damage mitochondrial DNA due to its vulnerable structure and may lead to mitochondrial dysfunctions including mitochondrial DNA mutations and reduction in ATP production and mitochondrial membrane potential that could cause age-related pathologies and death.[64,72,73] Although creating larger mitochondria organelles, fusion regulated by the Mfn1, Mfn2, and OPA1 proteins, the last of which is possibly expressed in photoreceptors,[74,75] mixes mitochondrial contents and dilutes minimally damaged components among normal organelles. While creating smaller mitochondria, fission regulated by Drp1 sequesters irreparably damaged mitochondrial components for repair or degradation by mitophagy.[62] This process involves transport toward the soma, consistent with our observation of mitochondria translocation to the cone soma as IS shorten. Chronic fission is an early event in cell death resulting from persisting oxidative stress.[64] An increase in oxidative stress is present in mitochondrial optic neuropathies.[68] Mitochondrial dysfunctions are common in the pathogenesis of neurodegenerative diseases such as Alzheimer, Parkinson, and Huntington diseases, and amyotrophic lateral sclerosis. Our observations provide a first glimpse of apparent mitochondrial dynamism in degenerating cones in human macula.

CONCLUSIONS

This hypothesis-generating study had limitations. Transmission electron microscopy and most histological analysis used single sections only. Despite short time between death and preservation compared to most studies using human tissues, mitochondria morphology was not optimal. However, animal models commonly used to study photoreceptor degeneration do not have a cone-rich fovea for color and high-acuity vision[27] or photoreceptors with long Henle fibers typical of human macula. Premortem clinical imaging was not available for the eyes in this study. Nonetheless, our data provide a context for our separate descriptions of cone degeneration in ORT[7,52] and overall fill a critical gap in the knowledge base for high-resolution clinical imaging. Furthermore, because TEM is comprehensive, our data also provide a context for targeted localizations afforded by selective markers like antibodies. In addition to imaging implications, our data provide new impetus for investigating the neurodegeneration of AMD at subcellular and molecular levels. As seen by TEM, mitochondria shrink and migrate toward the cone nucleus in degenerating cones both inside and outside ORT and are likely a major source of reflectivity observed with SD-OCT. Inner segments undergo substantial remodeling as degeneration proceeds. Our ability to follow photoreceptor degeneration in longitudinal studies of patient populations is now newly improved. Thus, photoreceptors can serve as accurate reporters of the signals coming from their support system (RPE and choroid) as it fails in AMD.

Disclosure: **K.M. Litts**, None; **J.D. Messinger**, None; **K.B. Freund**, None; **Y. Zhang**, None; **C.A. Curcio**, None

References

1. Johnson PT, Lewis GP, Talaga KC, et al. Drusen-associated degeneration in the retina. *Invest Ophthalmol Vis Sci*. 2003; 44:4481–4488.

2. Shelley EJ, Madigan MC, Natoli R, Penfold PL, Provis JM. Cone degeneration in aging and age-related macular degeneration. *Arch Ophthalmol*. 2009;127:483–492.

3. Johnson PT, Brown MN, Pulliam BC, Anderson DH, Johnson LV. Synaptic pathology, altered gene expression, and degeneration in photoreceptors impacted by drusen. *Invest Ophthalmol Vis Sci*. 2005;46:4788–4795.

4. Dunaief JL, Dentchev T, Ying GS, Milam AH. The role of apoptosis in age-related macular degeneration. *Arch Ophthalmol*. 2002;120:1435–1442.

5. Curcio CA, Medeiros NE, Millican CL. Photoreceptor loss in age-related macular degeneration. *Invest Ophthalmol Vis Sci*. 1996;37:1236–1249.

6. Zweifel SA, Engelbert M, Laud K, Margolis R, Spaide RF, Freund KB. Outer retinal tubulation: a novel optical coherence tomography finding. *Arch Ophthalmol*. 2009;127:1596–1602.

7. Schaal KB, Freund KB, Litts KM, Zhang Y, Messinger JD, Curcio CA. Outer retinal tubulation in advanced age-related macular degeneration: optical coherence tomographic findings correspond to histology [published online ahead of print January 29, 2015]. *Retina*. doi:10.1097/IAE.0000000000000471.

8. Williams DR. Imaging single cells in the living retina. *J Vis*. 2011;51(13):1379–1396.

9. Duncan JL, Zhang Y, Gandhi J, et al. High-resolution imaging with adaptive optics in patients with inherited retinal degeneration. *Invest Ophthalmol Vis Sci*. 2007;48:3283–3291.

10. Zayit-Soudry S, Duncan JL, Syed R, Menghini M, Roorda AJ. Cone structure imaged with adaptive optics scanning laser ophthalmoscopy in eyes with nonneovascular age-related macular degeneration. *Invest Ophthalmol Vis Sci*. 2013;54: 7498–7509.

11. Zhang Y, Wang X, Rivero EB, et al. Photoreceptor perturbation around subretinal drusenoid deposits as revealed by adaptive optics scanning laser ophthalmoscopy. *Am J Ophthalmol*. 2014;158:584–596.

12. Putnam NM, Hammer DX, Zhang Y, Merino D, Roorda A. Modeling the foveal cone mosaic imaged with adaptive optics scanning laser ophthalmoscopy. *Opt Express*. 2010;18:24902–24916.

13. Spaide RF, Curcio CA. Anatomical correlates to the bands seen in the outer retina by optical coherence tomography: literature review and model. *Retina*. 2011;31:1609–1619.

14. Hoang QV, Linsenmeier RA, Chung CK, Curcio CA. Photoreceptor inner segments in monkey and human retina: mitochondrial density, optics, and regional variation. *Vis Neurosci*. 2002;19:395–407.

15. Staurenghi G, Sadda S, Chakravarthy U, Spaide RF; International Nomenclature for Optical Coherence Tomography (IN-OCT) Panel. Proposed lexicon for anatomic landmarks in normal posterior segment spectral-domain optical coherence tomography: the IN-OCT consensus. *Ophthalmology*. 2014; 121:1572–1578.

16. Jonnal RS, Kocaoglu OP, Zawadzki RJ, Lee SH, Werner JS, Miller DT. The cellular origins of the outer retinal bands in optical coherence tomography images. *Invest Ophthalmol Vis Sci*. 2014;55:7904–7918.

17. Tychinsky V. The metabolic component of cellular refractivity and its importance for optical cytometry. *J Biophotonics*. 2009;2:494–504.

18. Rudnicka AR, Jarrar Z, Wormald R, Cook DG, Fletcher A, Owen CG. Age and gender variations in age-related macular degeneration prevalence in populations of European ancestry: a meta-analysis. *Ophthalmology*. 2012;119:571–580.

19. Xu GZ, Li WW, Tso MO. Apoptosis in human retinal degenerations. *Trans Am Ophthalmol Soc*. 1996;94:411–430; discussion 430.

20. Kim SY, Sadda S, Pearlman J, et al. Morphometric analysis of the macula in eyes with disciform age-related macular degeneration. *Retina*. 2002;22:471–477.

21. Kim SY, Sadda S, Humayun MS, de Juan E Jr, Melia BM, Green WR. Morphometric analysis of the macula in eyes with geographic atrophy due to age-related macular degeneration. *Retina*. 2002;22:464–470.

22. Bird AC, Phillips RL, Hageman GS. Geographic atrophy: a histopathological assessment. *JAMA Ophthalmol*. 2014;132:338–345.

23. Guyton JR, Klemp KF. Ultrastructural discrimination of lipid droplets and vesicles in atherosclerosis: value of osmium-thiocarbohydrazide-osmium and tannic acid-paraphenylenediamine techniques. *J Histochem Cytochem*. 1988;36:1319–1328.

24. Curcio CA, Millican CL, Bailey T, Kruth HS. Accumulation of cholesterol with age in human Bruch's membrane. *Invest Ophthalmol Vis Sci*. 2001;42:265–274.

25. Curcio CA, Messinger JD, Sloan KR, Mitra A, McGwin G, Spaide RF. Human chorioretinal layer thicknesses measured in macula-wide, high-resolution histologic sections. *Invest Ophthalmol Vis Sci*. 2011;52:3943–3954.

26. Curcio CA, Messinger JD, Sloan KR, McGwin G, Medeiros NE, Spaide RF. Subretinal drusenoid deposits in non-neovascular age-related macular degeneration: morphology, prevalence, topography, and biogenesis model. *Retina*. 2013;33:265–276.

27. Curcio CA, Sloan KR, Kalina RE, Hendrickson AE. Human photoreceptor topography. *J Comp Neurol*. 1990;292:497–523.

28. Curcio CA, Medeiros NE, Millican CL. The Alabama age-related macular degeneration grading system for donor eyes. *Invest Ophthalmol Vis Sci*. 1998;39:1085–1096.

29. Curcio CA, Presley JB, Millican CL, Medeiros NE. Basal deposits and drusen in eyes with age-related maculopathy: evidence for solid lipid particles. *Exp Eye Res*. 2005;80:761–775.

30. Wolff B, Matet A, Vasseur V, Sahel JA, Mauget-Faysse M. En face OCT imaging for the diagnosis of outer retinal tubulations in age-related macular degeneration. *J Ophthalmol*. 2012;2012:542417.

31. Polyak S. *The Retina*. Chicago: University of Chicago; 1941.

32. Nag TC, Wadhwa S, Chaudhury S. The occurrence of cone inclusions in the ageing human retina and their possible effect upon vision: an electron microscope study. *Brain Res Bull*. 2006;71:224–232.

33. Curcio CA, Millican CL, Allen KA, Kalina RE. Aging of the human photoreceptor mosaic: evidence for selective vulnerability of rods in central retina. *Invest Ophthalmol Vis Sci*. 1993;34:3278–3296.

34. Iwasaki M, Inomata H. Lipofuscin granules in human photoreceptor cells. *Invest Ophthalmol Vis Sci*. 1988;29:671–679.

35. Tucker GS. Refractile bodies in the inner segments of cones in the aging human retina. *Invest Ophthalmol Vis Sci*. 1986;27:708–715.

36. Spaide RF, Curcio CA. Drusen characterization with multimodal imaging. *Retina*. 2010;30:1441–1454.

37. Oak AS, Messinger JD, Curcio CA. Subretinal drusenoid deposits: further characterization by lipid histochemistry. *Retina*. 2014;34:825–826.

38. Meadway A, Girkin CA, Zhang Y. A dual-modal retinal imaging system with adaptive optics. *Opt Express*. 2013;21:29792–29807.

39. Miller DT, Kocaoglu OP, Wang Q, Lee S. Adaptive optics and the eye (super resolution OCT). *Eye*. 2011;25:321–330.

40. Zhang Y, Cense B, Rha J, et al. High-speed volumetric imaging of cone photoreceptors with adaptive optics spectral-domain optical coherence tomography. *Opt Express*. 2006;14:4380–4394.

41. Hermann B, Fernandez EJ, Unterhuber A, et al. Adaptive-optics ultrahigh-resolution optical coherence tomography. *Opt Lett*. 2004;29:2142–2144.

42. Panorgias A, Zawadzki RJ, Capps AG, Hunter AA, Morse LS, Werner JS. Multimodal assessment of microscopic morphology and retinal function in patients with geographic atrophy. *Invest Ophthalmol Vis Sci*. 2013;54:4372–4384.

43. Zawadzki RJ, Jones SM, Olivier SS, et al. Adaptive-optics optical coherence tomography for high-resolution and high-speed 3D retinal in vivo imaging. *Opt Express*. 2005;13:8532–8546.

44. Roorda A, Romero-Borja F, Donnelly Iii W, Queener H, Hebert T, Campbell M. Adaptive optics scanning laser ophthalmoscopy. *Opt Express*. 2002;10:405–412.

45. Zhang Y, Poonja S, Roorda A. MEMS-based adaptive optics scanning laser ophthalmoscopy. *Opt Lett*. 2006;31:1268–1270.

46. Burns SA, Tumbar R, Elsner AE, Ferguson D, Hammer DX. Large-field-of-view, modular, stabilized, adaptive-optics-based scanning laser ophthalmoscope. *J Opt Soc Am A Opt Image Sci Vis*. 2007;24:1313–1326.

47. Chen DC, Jones SM, Silva DA, Olivier SS. High-resolution adaptive optics scanning laser ophthalmoscope with dual deformable mirrors. *J Opt Soc Am A Opt Image Sci Vis*. 2007;24:1305–1312.

48. Mitamura Y, Mitamura-Aizawa S, Katome T, et al. Photoreceptor impairment and restoration on optical coherence tomographic image. *J Ophthalmol*. 2013;2013:518170.

49. Jung JJ, Freund KB. Long-term follow-up of outer retinal tubulation documented by eye-tracked and en face spectral-domain optical coherence tomography. *Arch Ophthalmol*. 2012;130:1618–1619.

50. Schuman SG, Koreishi AF, Farsiu S, Jung SH, Izatt JA, Toth CA. Photoreceptor layer thinning over drusen in eyes with age-related macular degeneration imaged in vivo with spectral-domain optical coherence tomography. *Ophthalmology*. 2009;116:488–496, e482.

51. Shields CL, Kaliki S, Rojanaporn D, Ferenczy SR, Shields JA. Enhanced depth imaging optical coherence tomography of small choroidal melanoma: comparison with choroidal nevus. *Arch Ophthalmol*. 2012;130:850–856.

52. Litts KM, Messinger JD, Dellatorre K, Yannuzzi LA, Freund KB, Curcio CA. Clinicopathological correlation of outer retinal tubulation in age-related macular degeneration [published online ahead of print March 10, 2015]. *JAMA Ophthalmol*. doi:10.1001/jamaophthalmol.2015.126

53. Wilson JD, Bigelow CE, Calkins DJ, Foster TH. Light scattering from intact cells reports oxidative-stress-induced mitochondrial swelling. *Biophys J*. 2005;88:2929–2938.

54. Wilson JD, Cottrell WJ, Foster TH. Index-of-refraction-dependent subcellular light scattering observed with organelle-specific dyes. *J Biomed Opt*. 2007;12:014010.

55. Mullins RF, Skeie JM, Malone EA, Kuehn MH. Macular and peripheral distribution of ICAM-1 in the human choriocapillaris and retina. *Mol Vis*. 2006;12:224–235.

56. Greenberg JP, Sherman J, Zweifel SA, et al. Spectral-domain optical coherence tomography staging and autofluorescence

imaging in achromatopsia. *JAMA Ophthalmol*. 2014;132:437–445.

57. Burke TR, Yzer S, Zernant J, Smith RT, Tsang SH, Allikmets R. Abnormality in the external limiting membrane in early Stargardt disease. *Ophthalmic Genet*. 2013;34:75–77.

58. Lee W, Noupuu K, Oll M, et al. The external limiting membrane in early-onset Stargardt disease. *Invest Ophthalmol Vis Sci*. 2014;55:6139–6149.

59. Young RW. Pathophysiology of age-related macular degeneration. *Surv Ophthalmol*. 1987;31:291–306.

60. Lyamzaev KG, Nepryakhina OK, Saprunova VB, et al. Novel mechanism of elimination of malfunctioning mitochondria (mitoptosis): formation of mitoptotic bodies and extrusion of mitochondrial material from the cell. *Biochim Biophys Acta*. 2008;1777:817–825.

61. Nakajima A, Kurihara H, Yagita H, Okumura K, Nakano H. Mitochondrial Extrusion through the cytoplasmic vacuoles during cell death. *J Biol Chem*. 2008;283:24128–24135.

62. MacAskill AF, Kittler JT. Control of mitochondrial transport and localization in neurons. *Trends Cell Biol*. 2010;20:102–112.

63. Bossy-Wetzel E, Barsoum MJ, Godzik A, Schwarzenbacher R, Lipton SA. Mitochondrial fission in apoptosis, neurodegeneration and aging. *Curr Opin Cell Biol*. 2003;15:706–716.

64. Knott AB, Perkins G, Schwarzenbacher R, Bossy-Wetzel E. Mitochondrial fragmentation in neurodegeneration. *Nat Rev Neurosci*. 2008;9:505–518.

65. Chen H, Chan DC. Mitochondrial dynamics—fusion, fission, movement, and mitophagy—in neurodegenerative diseases. *Hum Mol Genet*. 2009;18:R169–R176.

66. Chen H, Chan DC. Critical dependence of neurons on mitochondrial dynamics. *Curr Opin Cell Biol*. 2006;18:453–459.

67. Federico A, Cardaioli E, Da Pozzo P, Formichi P, Gallus GN, Radi E. Mitochondria, oxidative stress and neurodegeneration. *J Neurol Sci*. 2012;322:254–262.

68. Maresca A, la Morgia C, Caporali L, Valentino ML, Carelli V. The optic nerve: a "mito-window" on mitochondrial neurodegeneration. *Mol Cell Neurosci*. 2013;55:62–76.

69. McInnes J. Insights on altered mitochondrial function and dynamics in the pathogenesis of neurodegeneration. *Transl Neurodegenr*. 2013;2:12.

70. Youle RJ, van der Bliek AM. Mitochondrial fission, fusion, and stress. *Science*. 2012;337:1062–1065.

71. Pathak D, Berthet A, Nakamura K. Energy failure: does it contribute to neurodegeneration? *Ann Neurol*. 2013;74:506–516.

72. Balaban RS, Nemoto S, Finkel T. Mitochondria, oxidants, and aging. *Cell*. 2005;120:483–495.

73. Westermann B. Mitochondrial fusion and fission in cell life and death. *Nat Rev Mol Cell Biol*. 2010;11:872–884.

74. Wang AG, Fann MJ, Yu HY, Yen MY. OPA1 expression in the human retina and optic nerve. *Exp Eye Res*. 2006;83:1171–1178.

75. Pesch UE, Fries JE, Bette S, et al. OPA1, the disease gene for autosomal dominant optic atrophy, is specifically expressed in ganglion cells and intrinsic neurons of the retina. *Invest Ophthalmol Vis Sci*. 2004;45:4217–4225.